

超声波塑料焊接机理

张宗波¹, 王晓东², 罗 怡², 郑英松¹, 张彦国¹, 王立鼎²

(1. 大连理工大学 精密与特种加工教育部重点实验室, 辽宁 大连 116024

2. 大连理工大学 辽宁省微纳米技术及系统重点实验室, 辽宁 大连 116024)

摘 要: 采用数值仿真和试验研究了超声波塑料焊接过程中不同特征温度段的产热机理. 利用有限元法 (FEM) 对聚甲基丙烯酸甲酯 (PMMA) 材料超声波焊接过程中的粘弹性热以及摩擦热进行了计算. 基于计算结果, 提出了摩擦热是焊接过程的启动热源, 粘弹性热是焊接过程主要热源的观点. 制备了相应的试件并搭建测温系统对焊接过程进行测温试验, 试验结果验证了仿真结果的正确性. 对焊接过程中的产热机理给出了更清晰的解释, 有助于超声波塑料焊接技术进一步在精密焊接领域的应用.

关键词: 超声波焊接; 粘弹性热; 有限元

中图分类号: TH6 **文献标识码:** A **文章编号:** 0253-360X(2010)11-0029-04



张宗波

0 序 言

超声波塑料焊接具有不需要焊剂和外部加热、时间短、强度高等诸多优点, 是塑料及其复合材料的重要连接方法. 近年来, 越来越多的研究者将该技术应用到精密焊接领域如聚合物微/纳机电 (M/NMES) 器件的连接封装等^[1], 这为该技术提供了更广阔的应用前景, 同时也对焊接产热机理的认识提出了更高的要求. 关于超声波焊接机理, 国内外进行了大量的试验研究与理论分析^[2]. 早期人们普遍认为超声波塑料焊接是靠焊件接触表面间的摩擦产热而实现的熔融连接. 随着研究的深入, 人们逐渐发现粘弹性热是在超声波焊接中使材料熔融的主要热源^[3-5].

随着粘弹性理论和数值计算技术的发展, 仿真计算成为了解超声波焊接过程的有效手段. 许多研究者针对粘弹性热提出了相应的理论模型和数值计算方法^[4,6,7]. 然而, 目前大部分研究者对粘弹性热的计算是先根据简化的力学模型求解材料在焊接过程中的应变分布, 然后利用简化公式并通过外推损耗量 E 进行粘弹性热的计算, 这种方法引入了模型简化带来的误差. 在前期的工作中提出了一种基于直接模拟材料本构关系计算粘弹性热的仿真策略, 并验证了其有效性^[7]. 在超声波焊接过程中, 随

着温度的变化聚合物材料一般会经历玻璃态、过渡态、粘弹态和粘流态等不同的阶段. 聚合物材料在不同的状态下其力学特性相差很大, 所以有必要对不同特征温度段的产热机理进行分别研究.

文中以 PMMA 材料为例, 对超声波焊接过程中低于玻璃转化温度 (T_g) 和高于 T_g 的产热机理进行了数值计算和试验研究. 基于计算结果, 提出了超声波焊接过程中界面摩擦热是启动热源, 而粘弹性热是主要热源的观点. 进行了焊接测温试验, 结果验证了此观点的正确性.

1 仿真分析

1.1 仿真模型

以研究组前期提出的粘弹性热计算模型为基础^[7], 借助商用软件 Ansys 对 PMMA 材料超声波焊接中的产热过程进行了仿真计算. 为了提高计算效率采用二维模型, 如图 1 所示. 采用矩形导能筋结构, 与传统的点接触或线接触式导能筋相比面接触式的矩形导能筋有效的增加了初始接触面积, 能够减缓焊接的产热过程, 更有利于温度的测量和分析. PMMA 板材的材料参数为: 密度 1.18 kg/m^3 , 比热容 $1.47 \text{ J/(kg} \cdot \text{}^\circ\text{C)}$, 热导率 $0.2 \text{ mW/(mm} \cdot \text{K)}$. 选用 Visco88 粘弹性单元, 材料本构关系选择 10 单元广义 Maxwell 模型. 超声振动的振幅为 $18 \mu\text{m}$, 频率为 30 kHz 施加于模型的上表面, 底面节点为全约束. 为了说明不同起始温度对粘弹性热的影响, 分别选

取起始温度为 25 90 98 °C对粘弹性热进行计算.

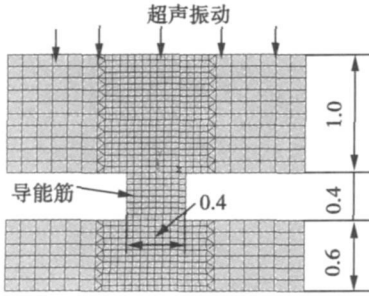


图 1 有限元计算模型 (mm)
Fig 1 Finite element model

利用瞬态热-结构直接耦合模型对材料处于玻璃态时的摩擦热进行了计算. 计算的起始温度为 25 °C, 界面摩擦系数为 0.4 选用 Plan23 直接耦合单元, 界面间采用罚函数法进行接触分析. 最后综合粘弹热与摩擦热的仿真过程, 提出了计及粘弹热、摩擦热以及热传导过程的仿真策略: 对每一个振动周期首先进行摩擦与热传导计算, 将所得的温度场作为粘弹热的初始温度场计算粘弹性热. 将粘弹热所得温度场作为下一个计算周期摩擦与热传导过程的初始温度, 循环计算直至达到所设定的计算周期数.

1.2 仿真结果分析

图 2 为起始温度分别为 25 °C和 90 °C时, 导能筋界面上一点由粘弹性热引起的温升曲线. 图中显示, 经过长达 0.2 s 的焊接, 温度的升高量小于 2 °C. 以这样的温升速率导能筋不可能像实际焊接过程那样在几秒甚至小于 1 s 的时间内熔融. 由图 2 中的两条曲线可以看出起始温度为 25 °C和 90 °C 时, 其温升速率和温升总量近似, 说明在这一温度范围内粘弹性产热速率随起始温度的变化不大. 因此, 在此温度段材料的粘弹性产热效应并不明显, 即

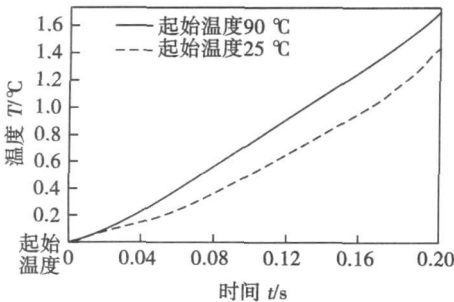


图 2 起始温度分别为 25 °C和 90 °C的粘弹热引起的温升曲线
Fig 2 Temperature curves caused by viscoelastic heat with initial temperatures of 25 °C and 90 °C

使施加长时间的超声也不足以使材料熔融甚至软化, 所以除粘弹性热以外在此温度段应该还存在其它产热机理.

图 3 为起始温度为 98 °C时导能筋界面上一点由粘弹性热引起的温升曲线. 图中显示, 在 T_g 附近温升速率存在明显的拐点, 在拐点处温升速率急剧升高, 致使材料在 0.02 s 内升高近 50 °C, 这一趋势与文献[5]中试验测得的升温趋势吻合. 因此在超声焊接过程中, 粘弹热需要一定的激活热量将材料加热到 T_g 附近才能明显的表现出来.

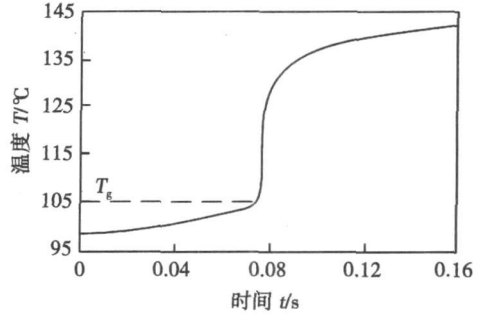


图 3 起始温度为 98 °C时粘弹热温升曲线
Fig 3 Temperature curve caused by viscoelastic heat with initial temperature of 98 °C

通过对焊接过程的瞬态分析可知, 在焊接过程中由于焊件特别是导能筋存在明显的形变, 在焊件与导能筋的接触面上会发生因应变引起的相对微滑移. 虽然滑移的绝对距离很小, 但是由于超声频率高, 所以最高滑移速度可达 532.463 mm/s, 摩擦应力高达 12.252 MPa. 仿真结果显示, 滑移速率的最大点出现在导能筋表面的角点位置, 随着与角点距离的增加, 导能筋表面上各点的滑移速率逐渐减小, 在导能筋表面的中心位置滑移速率几乎为 0. 当摩擦系数为 0.4 时, 经计算得导能筋角点的功率密度为 6.52 W/mm², 这足以使局部材料的温度在较短的时间内升至较高值. 进一步利用热-结构直接耦合模型对这一过程的摩擦热进行计算, 结果如下: 摩擦热产生的温度峰值出现在导能筋表面的角点位置, 而且随着与角点距离的增加温度逐渐减小, 如图 4 所示, 这与相对滑移速率的分布规律相符. 提取导能筋上的角点 (点 1), 角点附近一点 (点 3) 和角点附近下焊件上一点 (点 2) 的温升曲线, 如图 5 所示. 结果显示, 角点的温度在 0.1 s 内可升高近 80 °C, 而且越靠近角点温升越快. 综合考虑摩擦热、热传导以及粘弹热时, 经过 0.2 s 焊接导能筋上的温度分布如图 6 所示.

由仿真结果可知, 摩擦热是超声焊接的启动热,

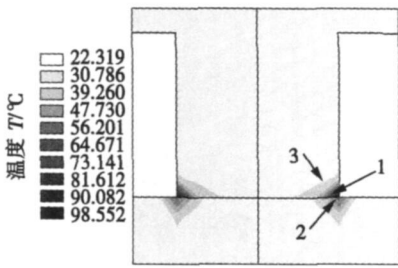


图 4 摩擦热引起的温度场分布

Fig. 4 Temperature distribution caused by facial friction

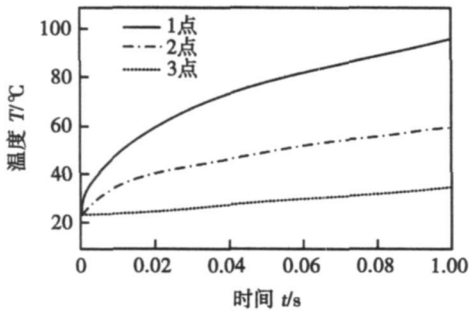


图 5 摩擦热引起的导能筋上不同点的温升曲线

Fig. 5 Temperature curves caused by friction at different locations

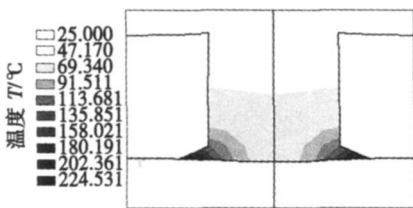


图 6 考虑摩擦热计算和热传导以及粘弹热的温度场分布

Fig. 6 Simulation result of temperature distribution and deformation of energy director

对于矩形导能筋摩擦热会从导能筋的角点产生, 所以角点的温升应快于其它部位. 随着温度继续升高, 角点处的部分材料温度达到 T_g 附近. 根据上面关于粘弹性产热机理的分析, 此时粘弹性产热过程会被激活, 温度迅速升高, 从而与其周围的材料在短时间内产生较大的温度梯度. 在热传导作用下其周围的材料也会逐渐到达 T_g 而激活粘弹热. 随着超声焊接过程的继续, 此传热和粘弹性产热过程会使热影响区迅速扩大, 从而使导能筋发生熔融和变形, 实现器件间的连接.

2 测温试验

粘弹热是一种体热, 与应力应变的分布有关, 而

与界面的有无没有关系. 为了考察界面摩擦效应对焊接过程的影响, 分别制作了尺寸相同的带矩形导能筋的无界面和有界面试件, 如图 7 所示, 如果焊接参数相同那么焊接过程中试件的应力应变分布是相同的, 可以通过两种试件中温度场的差别反映界面摩擦对温升过程的影响.

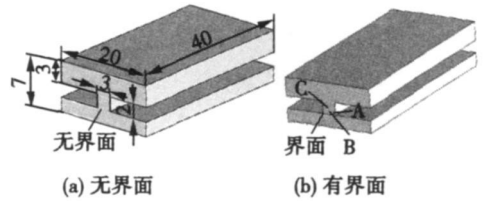


图 7 试件示意图 (mm)

Fig. 7 Schematic of specimens

试件由 PMMA 板材加工制成, 材料的 T_g 为 $105\text{ }^\circ\text{C}$. 温度测量选用美国 OMEGA 公司生产的 TT-K-36-SLE 型微细热电偶, 线芯直径为 0.127 mm , 热电偶响应时间约为 0.1 ms . 热电偶在测量范围内的输出电压为 $0\sim 10\text{ mV}$ 而数据采集卡的量程为 $0\sim 10\text{ V}$ 因此选用 AD524 放大器, 将信号放大 1 000 倍后传输给采集卡. 采集卡选用 NI DAQPad-6015 3 通道模拟输入, 单路采样频率为 50 kHz . 由于热电偶是温差传感器, 在测量中还要记录下热电偶冷端的温度 T_c . 基于 LabVIEW 软件编写了高速数据采集和处理程序. 分别将热电偶埋置于导能筋的下表面角点 A、下表面中心点 B 以及导能筋中点 C 处, 见图 7. 试验所用焊机为 Branson 2000X ψ aef 型系列焊机, 频率为 30 kHz 焊接力设为 100 N 振幅为 $18\text{ }\mu\text{m}$.

3 结果与讨论

图 8 为无界面试件的超声焊接温度曲线, 经过长达 2 s 焊接测点的最高温升仅为 $20\text{ }^\circ\text{C}$ 左右, 远未达到材料的软化温度, 不可能熔融形成焊区. 焊接结束后, 试件与工具头接触的表面有烧伤痕迹, 且测点中越靠近上表面温升越明显, 因此可以推断所测得的温升主要从上表面热传导而来.

图 9 为有界面试件焊接过程中的温度曲线, 图中显示导能筋角点 A 的温度升高要快于其它两点. A 点与 B 点的温升规律相似, 在前期温升速率较慢, 角点 A 的最大温升速率为 $267\text{ }^\circ\text{C/s}$ 在上面的仿真计算中最快温升为 $390\text{ }^\circ\text{C/s}$ 这一温升速率与仿真结果中摩擦热的产热速率数量级吻合但略低于仿真结果, 这主要是由于仿真计算中没有考虑向空气中

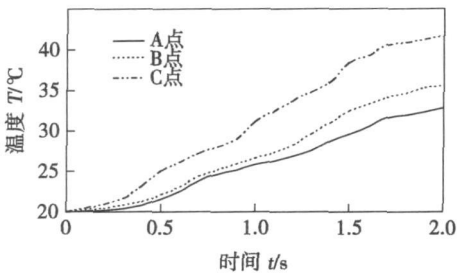


图 8 无界面试件中各点的温度曲线

Fig 8 Temperature curves of specimen without interface

的热辐射,而且试验中角点的位置并不是理想的角点位置,而仿真结果角点位置则是严格意义上的导能筋左下角节点。B点受界面效应的影响也存在摩擦热,但由仿真结果可知它与底面的相对滑动小于A点,所以其温升速率也较A点小,但是由于界面上由角点A开始向B点逐渐变热,摩擦和热传导作用使B点持续升温。

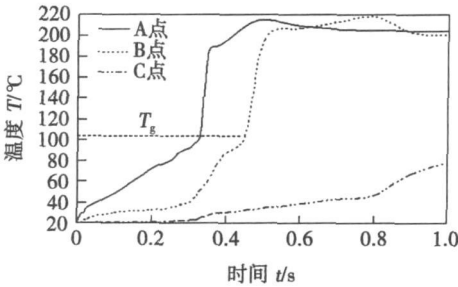


图 9 有界面试件中各点的温度曲线

Fig 9 Temperature curves of specimen with interface

A点和B点的温升曲线在 T_g 附近都存在明显的拐点,在温度高于 T_g 后的0.025 s内温度迅速升高近70°C,仿真结果中粘弹热使温度在0.02 s内升高近50°C,仿真结果与试验测量结果非常吻合,具有典型的高于 T_g 的粘弹性产热特征。而C点由于离界面较远,所以只有很少的热量传导到C点,焊接2 s后由于导能筋的坍塌和大量材料温度到达 T_g 后产生较多的粘弹热,在热传导作用下使C点的温度开始明显升高。比较两种试件的测温结果可知,在有界面的试件中A点与B点分别在前0.3 s和0.5 s上升了80°C,而图8中在相同的荷载下其温度升高量较小。所以可以证明,前期的这部分热量主要不是来源于粘弹性热,而界面的有无是决定这部分热量有无的关键,结合仿真结果和上面的分

析可知这部分热量主要来源于界面的摩擦热。

4 结 论

(1)所使用的数值计算方法可以较准确地对超声波焊接过程中的摩擦热和粘弹热进行计算。

(2)在超声波塑料焊接过程中界面摩擦热是该过程的启动热源,没有界面摩擦焊接过程就无法开始;而粘弹热是焊接过程的主要热源。文中研究对超声波塑料焊接的产热过程给出了更清晰的解释,有助于进一步对不同温度范围内温升机理进行利用和控制。

参考文献:

- [1] Truckemüller R, Ahrens R. An ultrasonic welding based process for building up a new class of inert fluidic micro sensors and actuators from polymers [J]. *Sensors and Actuators A* 2006, 132(1): 385-392.
- [2] 张宗波, 罗 怡, 王晓东, 等. 塑料超声波焊接及其用于聚合物 MEMS器件键合的研究进展 [J]. *焊接*, 2008(8): 9-15. Zhang Zongbo, Luo Yi, Wang Xiaodong, et al. Advances in ultrasonic welding of plastics and its usage in polymer MEMS bonding [J]. *Welding & Joining* 2008(8): 9-15.
- [3] Tolunary M N, Dawson P B, Wang K K. Heating and bonding mechanisms in ultrasonic welding of thermoplastics [J]. *Polymer Engineering and Science* 1983, 23(13): 726-733.
- [4] Benatar A, Timothy Gorwshi G. Ultrasonic welding of PEEK/graphite APC-2 composites [J]. *Polymer Engineering and Science* 1989, 29(23): 1705-1721.
- [5] Frankele J, Wang K K. Energy transfer and bond strength in ultrasonic welding of thermoplastics [J]. *Polymer Engineering and Science* 1980, 20(6): 396-401.
- [6] Xiaolin W, Jiaochun Y, Ruiqi L, et al. FEM investigation of the temperature field of energy director during ultrasonic welding of PEEK [J]. *Journal of Thermoplastic Composite Material* 2006, 19(9): 593-607.
- [7] 张振强, 张宗波, 罗 怡, 等. 超声波塑料焊接粘弹性热的仿真计算 [J]. *焊接学报*, 2009, 30(9): 97-100. Zhang Zhengqiang, Zhang Zongbo, Luo Yi, et al. Simulation of viscoelastic heat during ultrasonic welding of thermoplastics [J]. *Transactions of the China Welding Institution* 2009, 30(9): 97-100.

作者简介: 张宗波,男,1982年出生,博士研究生,主要从事微纳器件制造研究工作,发表论文20余篇。

E-mail: z4001_0@163.com

ingful. Furthermore, discussions about radial distributions of VPPA pressure can actually guide mechanical analysis and numerical simulation of VPPA and its molten pool. In this paper, the distribution of VPPA pressure along the radial distance at different welding currents was measured and discussed by U-tube barometer. It was concluded that the radial distribution of VPPA pressure still belonged to Gaussian distribution rather than exponential distribution. Furthermore, the analyzed results show that the VPPA pressure increases with the increase of welding current, but its increasing rate tends to slow.

Key words: variable polarity plasma arc welding; arc pressure; U-tube barometer; radial distribution

Weld defect detection of double sides weld based on X-ray digitized image SHAO Jaxin, DU Dong, ZHU Xinjie, GAO Zhilong, WANG Chen (1. Key Laboratory for Advanced Materials Processing Technology, Ministry of Education, Tsinghua University, Beijing 100084, China; 2. North China Petroleum Steel Pipe Co., Ltd. Qinxiang 062650, Hebei, China), P 21—24

Abstract: The automatic detection of weld defects based on image processing of X-ray digitized film is important in the engineering field. Ideas of respectively processing the weld edge area and the other area of weld and respectively processing the slim line defects and the other defects were proposed for automatic detection of the double sides weld defects. The outer edges and the edges of the overlapped area of double sides weld were segmented by grey waveform analysis with column by column. And then the large templates of median filter and mean filter were combined to simulate the weld background, and the weld defects were detected by segment threshold after the background being subtracted. The algorithms of adaptive image binarization with column by column and modified Hough transform were proposed to detect the slim line defects. The result shows that the proposed algorithm avoids false alarms on the edges of the overlapped area for the double sides weld and weak line defects are detected effectively.

Key words: X-ray inspection; double sides weld; weld defect; image processing

Analysis on laser arc hybrid welded joint of high strength steel JFE980S by thermal simulation test WANG Xuyou, TENG Bin, LEI Zhen, LN Shangyang (Harbin Welding Institute, China Academy of Machinery Science & Technology, Harbin 150080, China), P 25—28

Abstract: The brittleness and softening of HAZ of high strength steel JFE980S were studied by thermal simulation test. After the thermal cycle curve of laser hybrid welding and MAG welding being measured, the HAZ of two welding methods were simulated by means of the thermal simulation machine of Gleeb3500, and the microstructure, tensile strength and the impact toughness at -20 °C of the specimens were tested and analyzed. The results indicate that the residence time of peak temperature, $t_{8/5}$ and $t_{5/3}$ in laser arc hybrid welding are all less than those in MAG welding. The impact toughness of the coarse grained region in joint by hybrid welding is as two times high as that by MAG welding. The tensile strength of the incomplete

Phase transformation region was increased by more than 100 MPa, which was compared with the common MAG welding.

Key words: hybrid welding; thermal simulation; brittleness; softening; high strength steel

Ultrasonic welding mechanism of thermoplastics and its thermal process ZHANG Zongbo, WANG Xiaodong, LUO Yi, ZHENG Yingsong, ZHANG Yanguo, WANG Lidong (1. Key Laboratory for Micro/Nano Technology and System of Liaoning Province, Dalian 116024, Liaoning, China; 2. Key Laboratory for Precision and Non-traditional Machining Technology of Ministry of Education, Dalian University of Technology, Dalian 116024, Liaoning, China), P 29—32

Abstract: Heat production mechanisms in temperature ranges below and above T_g (glass transition temperature) of thermoplastic components were studied by numerical simulation and experiment. The viscoelastic heat and facial friction heat in ultrasonic welding of PMMA (poly(methyl methacrylate)) were numerically calculated by FEM (Finite Element Method). Temperature was measured to verify the simulation results. Results of simulation and experiment agree well with each other, which indicate that the facial friction heat is the initial heat source in ultrasonic welding process. Heat conduction effect chain reactively activates the generation of the viscoelastic heat when temperature reaches T_g of the base metal. And the viscoelastic heat provides most required heat during welding. The present study gives a more clear understanding of heat production mechanisms in ultrasonic welding.

Key words: ultrasonic welding; viscoelastic heat; finite element method

Analysis on joint softening for JFE980S high strength steel

LEI Zhen, WANG Xuyou, TENG Bin, ZHENG Hongyang (1. Harbin Welding Institute, China Academy of Machinery Science & Technology, Harbin 150080, China; 2. Heilongjiang Provincial Institute of Architectural Design and Research, Harbin 150008, China), P 33—37

Abstract: The softening problems in the joints of low alloy high strength steel JFE980S by laser/MAG hybrid welding and MAG welding were studied. The softening law and mechanism for the quenched and tempered low alloy high strength steel joints were discussed according to the results of tensile test, hardness test and microstructure analysis. The result indicated that the joints by MAG welding are seriously softened, but the joints by laser/MAG hybrid welding only are softened a little. And the softened zone width and the softened degree of the joints by laser/MAG hybrid welding are both smaller and lower than those of the joints by MAG welding. The softening mainly appears in over-tempering zone and incomplete normalizing zone in the HAZ. And the distribution of granular or nubby microstructure along the grain boundaries is the main reason of the softening.

Key words: quenched and tempered low alloy high strength steel; joint softening; laser/MAG arc hybrid welding

Numerical simulation of keyhole formation process in laser